

Article

Effect of Austenitizing Temperature on the Work Hardening Behavior of Air-Hardening Steel LH800

Xiang Luo ¹, Zhenli Mi ^{1,*}, Yanxin Wu ¹, Yonggang Yang ¹, Haitao Jiang ¹ and Kuanhui Hu ²

¹ Institute of Engineering Technology, University of Science and Technology Beijing, Beijing 100083, China; b20170467@xs.ustb.edu.cn (X.L.); wuyanxin@ustb.edu.cn (Y.W.); yangyg@ustb.edu.cn (Y.Y.); jianght@ustb.edu.cn (H.J.)

² Central Research Institute, Baoshan Iron & Steel Co., Ltd., Shanghai 201900, China; b20170564@xs.ustb.edu.cn

* Correspondence: mizl@necar.ustb.edu.cn

Abstract: In this paper, we present the effect of austenitizing temperature on the work hardening behavior of air-hardening steel LH800 by evaluating the influence of austenitizing temperature on microstructure evolution and mechanical properties, using Hollomon, Differential Crussard–Jaoul (D_{C-J}), and Modified C–J (M_{C-J}) work hardening models. The results reveal that with an increase in austenitizing temperature, there is an increase in the percentage of martensite, along with an increase in the strength and hardness of the LH800 steel; on the other hand, there is a decrease in the plasticity. Austenitized at 825 °C, LH800 steel exhibits its highest strength and good plasticity, with a tensile strength of 897 MPa and an elongation of 13.6%. The comparison between the three strain hardening models revealed that the Hollomon model was the finest fit for the experimental data utilized and could illustrate the work hardening behavior of LH800 steel most suitably. This model manifests a two-stage work hardening mechanism; the first stage is related to the plastic deformation of ferrite phase, while the second stage deals with the co-deformation of ferrite and martensite/bainite phase. As austenitizing temperature increases, the work hardening ability of LH800 steel diminishes at each stage, the transition strain decreases, and the plastic deformation of martensite starts earlier.

Keywords: air-hardening steel LH800; austenitizing temperature; mechanical properties; microstructure evolution; work hardening



Citation: Luo, X.; Mi, Z.; Wu, Y.; Yang, Y.; Jiang, H.; Hu, K. Effect of Austenitizing Temperature on the Work Hardening Behavior of Air-Hardening Steel LH800. *Metals* **2022**, *12*, 1026. <https://doi.org/10.3390/met12061026>

Academic Editor: Carlos Garcia-Mateo

Received: 17 May 2022

Accepted: 13 June 2022

Published: 16 June 2022

Publisher's Note: MDPI stays neutral with regard to jurisdictional claims in published maps and institutional affiliations.



Copyright: © 2022 by the authors. Licensee MDPI, Basel, Switzerland. This article is an open access article distributed under the terms and conditions of the Creative Commons Attribution (CC BY) license (<https://creativecommons.org/licenses/by/4.0/>).

1. Introduction

Dual phase (DP) steels are high-strength low-alloy steels comprising a hard martensitic phase and a soft ferrite matrix with good mechanical properties [1–3]. Formerly, DP steel had extensive applicability in the production of automotive steel due to its superior mechanical properties [4–6]. However, the advancement of the steel industry has led to the continual enhancement of the production and application strength grades of contemporary automotive steel. Traditional DP steel is unable to conform to the design and the other requirements of the latest automotive steel generation due to its limited strength. In recent years, air-hardening steel LH800 [7,8] has emerged, which exhibits conducive cold forming properties in the ferrite state, and it can be easily processed into a multitude of complex structural parts. High strength and good plasticity can be achieved for this steel by austenitization and air quenching to room temperature. LH800 is essentially a low-alloy steel with the addition of Mn, Cr, and Mo and trace element B based on traditional DP steel. The addition of Mn, Cr, Mo, and trace element B not only significantly strengthens the hardenability of the alloy steel and moves its C curve shift notably to the right, but it also boosts the strength of the alloy steel. The steel structural parts are strengthened by the heat treatment after being cold formed, while air-cooling speed is quite low. Therefore, the structural parts obtained by air quenching demonstrate less deformation, less rebound, more stable component size, and satisfactory performance [9,10].

In recent years, several German scholars conducted a series of studies on LH800 steel: Grydin et al. [7] analyzed the effect of pre-deformation and heat treatment on the LH800 steel. They derived an empirical formula for the influence of martensitic lath thickness and prior austenite grain size on yield strength, which served as a guide for the cold-formed modeling as well as the heat treatment process of LH800 steel. Schaper et al. [8] studied the microstructure evolution and property changes in LH800 steel while undergoing heat treatment and proposed a mathematical description illustrating the formation of martensite during the air-quench strengthening process. Grydin et al. [9] obtained martensite + ferrite dual-phase structure by austenitizing LH800 steel below the upper critical temperature (A_{c3}) and, thereby, established a relationship between its mechanical properties and microstructural parameters. For example, its tensile and yield strengths can be calculated using the mixed strength formula based on the percentage of martensite and ferrite phase. Nonetheless, the majority of the existing studies are focused on the changes in microstructure and mechanical properties of LH800 steel, while very few scholars expanded their research to further study its room temperature deformation mechanism and work hardening behavior characteristics.

This study primarily aims to elucidate the effect of martensite phase proportion differences caused by variations in austenitizing temperature on the deformation mechanism and work hardening behavior of LH800 steel. The work hardening behavior of LH800 steel was explored by implementing a mechanical properties test, Hollomon model, differential C-J model, and modified C-J model; thus, the plastic deformation mechanism of LH800 steel was determined.

2. Materials and Experimental Procedure

A low-alloy steel of composition (wt.%) 0.097 C, 1.83 Mn, 0.25 Si, 0.79 Cr, 0.15 Mo, 0.027 Ti, 0.057 V, 0.0047 B, 0.006 P and 0.003 S was used in this experiment. Firstly, the ingot was forged into a slab of a certain size, cut into smaller pieces, and then heated to 1200 °C and held at that temperature for 2 h. Next, it was hot rolled to 5 mm with a total reduction of 83.3% and held at 700 °C for 2 h to simulate coiling, with the furnace being cooled to room temperature, and finally cold rolled to 1.5 mm. Furthermore, it was kept at 700 °C for 4 h and cooled to room temperature to obtain a steel sheet in the as-supplied state. Subsequently, it was subjected to 5% pre-stretch deformation to stimulate cold forming. Finally, it was austenitized at different temperatures and kept for 15 min, followed by air quenching.

In order to design a reasonable austenitizing process, the A_{c1} and A_{c3} temperatures of the LH800 steel were measured first by employing a thermal dilatometer. The thermal expansion curve of the LH800 steel is shown in Figure 1, and the corresponding A_{c1} and A_{c3} temperatures were 726 °C and 850 °C, respectively. Subsequently, the 5% pre-strained steel sheet was heat-treated between A_{c1} and A_{c3} to evaluate the influence of austenitizing temperature on its work hardening behavior. The heat treatment process is shown in Figure 2.

The pre-strained steel plate that was strengthened by heat treatment was then cut by wire cutting along its rolling direction to take standard tensile samples (width 6 mm, thickness 1.5 mm, and gauge length 25 mm). The tensile properties were tested by using SANS CMT5105 electronic universal testing machine (CMT 5105, SANS, Shenzhen, China) with a loading speed of 1 mm/min. After grinding and polishing the heat-treated samples, they were etched with 4% nitric acid for about 3–5 s to prepare them as scanning electron microscope (SEM) samples. The microstructure of the samples was observed by employing scanning electron microscope (SEM, Quanta FEG 450, FEI Company, Hillsboro, OR, USA). The HMAS-D1000SM Vickers hardness tester (Shanghai Yanrun Optical Machine Technology Co., LTD, Shanghai, China) was utilized to test various heat-treated samples; each sample was tested with five data sets at different positions, and then their average value was considered. The percentages of martensitic phase and the ferrite grain size were measured using Image Pro Plus (Media Cybernetics, Inc., Rockville, Maryland, MD,

USA) and Photoshop (Adobe Systems Incorporated, San Jose, California, USA) Image processing software.

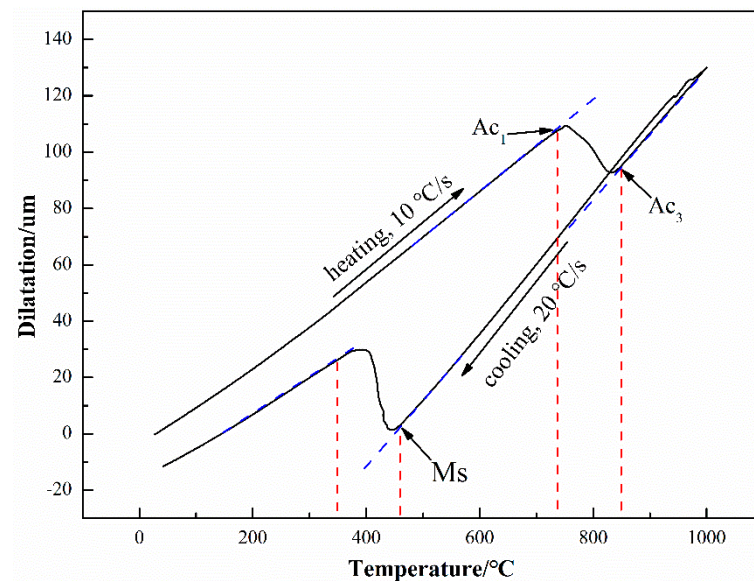


Figure 1. Dilatation vs. temperature curve of LH800 steel.

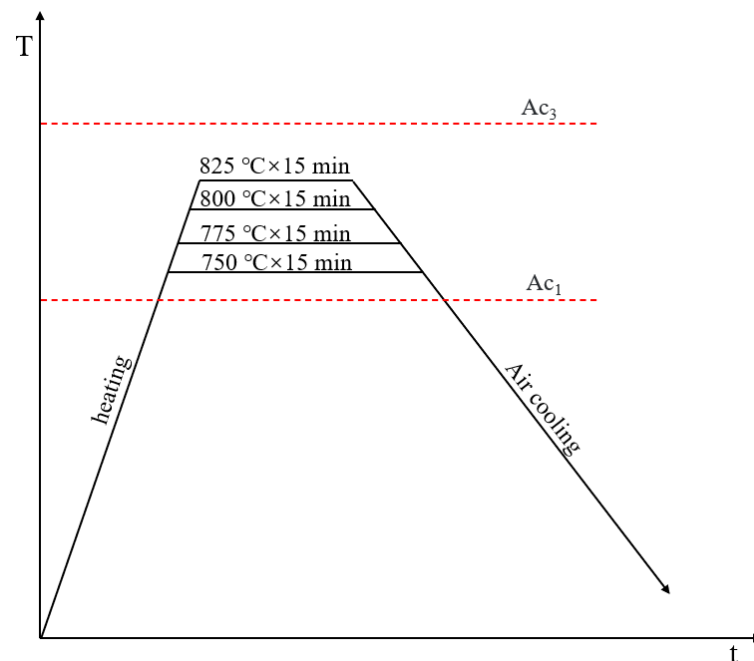


Figure 2. Schematic diagram of the heat treatment process of LH800 steel.

3. Results and Discussion

3.1. Initial Microstructure and Properties

Figure 3 demonstrates the microstructure of LH800 steel as cold rolled and as-supplied. Figure 3a clearly indicates that the cold-rolled structure of LH800 steel is predominantly composed of ferrite and pearlite. As shown in the figure, the white area denotes pearlite, while the gray area is ferrite. Figure 3b displays the microstructure of the cold-rolled steel, which was annealed at 700 °C for 4 h. The structure of the LH800 steel consists of ferrite + carbide and possesses equiaxed ferrite grains of different sizes. A large number of micro-scale carbides were distributed evenly along the ferrite grain boundaries, and a

small quantity of nano-sized carbides was distributed among the ferrite grains. Figure 4 depicts the engineering stress–strain curves of the cold-rolled and as-supplied steel. It can be observed that the engineering stress–strain curve of the cold-rolled state expresses continuous yielding, and its yield and tensile strength were found to be 1206 MPa and 1245 MPa, respectively, while the elongation was only 3.5%. Evidently, the tension curve of the supply state also reveals that, post annealing, the strength of the cold-rolled sheet shows a sharp decline, with elongation increasing significantly, inducing an apparent yield plateau. The yield and tensile strength at this point were 310 MPa and 458 MPa, respectively, and elongation was as high as 32%, which is beneficial to the subsequent cold forming process.

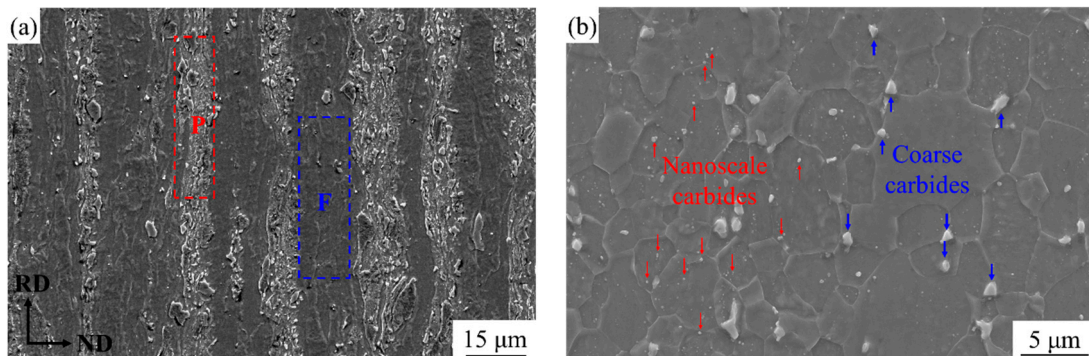


Figure 3. Initial microstructure of LH800 steel: (a) cold-rolled state and (b) as-supplied state. F: ferrite; P: pearlite; RD: rolling direction; ND: normal direction.

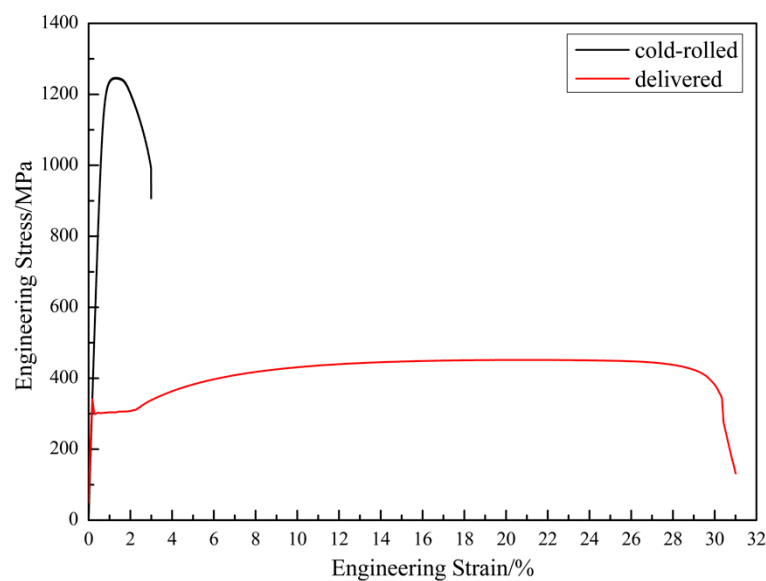


Figure 4. Engineering stress–strain curves of LH800 steel in cold-rolled and as-supplied state.

3.2. Microstructure Analysis

The as-supplied steel plate treated with 5% pre-strain was austenitized at various temperatures; its microstructure is shown in Figure 5. A dual-phase structure of ferrite + martensite was obtained between 750 °C and 800 °C, while the ferrite matrix contained a marginal amount of carbide. With the increase in holding temperature, the degree of austenitization increases, thereby increasing the percentage of martensite obtained by air quenching but reducing the percentage of ferrite; no substantial change occurred for the carbides in this matrix. When the austenitizing temperature reaches 825 °C, the multiphase structure of ferrite + granular bainite + martensite is achieved by air quenching, while the carbides in the ferrite matrix show a slight increase as well.

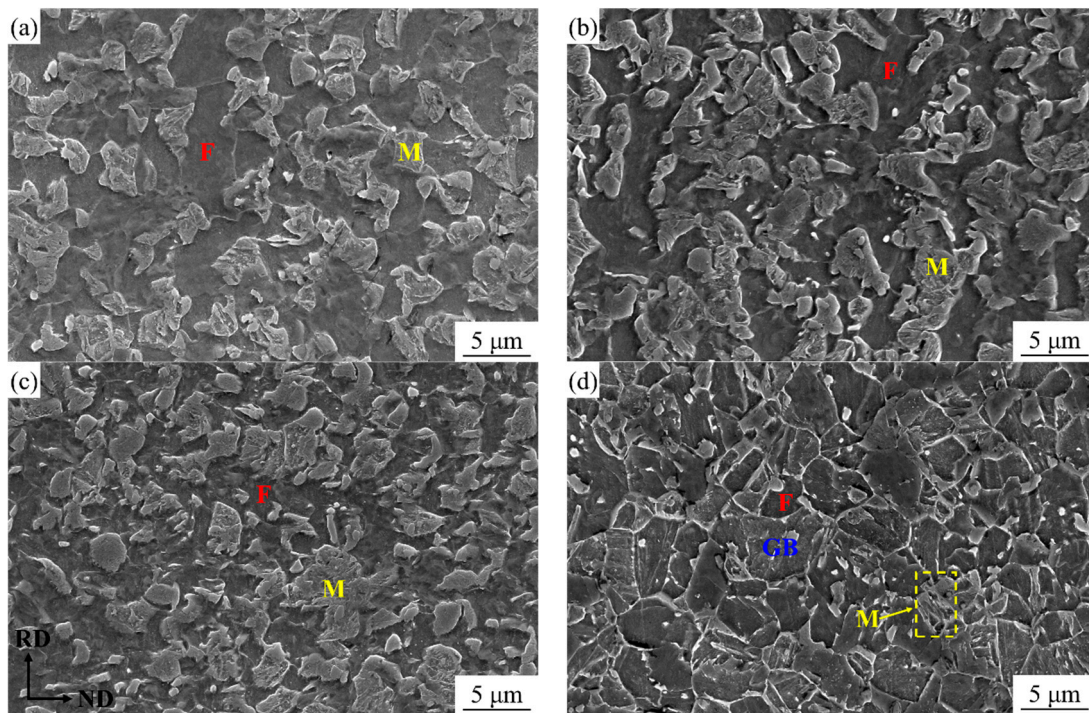


Figure 5. The microstructure of LH800 steel held at different temperatures for 15 min followed by air quenching: (a) 750 °C; (b) 775 °C; (c) 800 °C; (d) 825 °C. F: ferrite; M: martensite; GB: granular bainite; RD: rolling direction; ND: normal direction.

When the holding temperature is lower, the degree of austenitization is lower. Based on the carbon concentration balance in the steel, the austenitic carbon content appears to be higher during the austenitization process. Carbon is an austenite stabilizing element, which makes the experimental steel less prone to high and medium temperature transformation. Since Cr, Mn, B and certain other elements are added to the steel to enhance hardenability, the experimental steel can be austenitized below A_{c3} and martensitic structure can be obtained at a slower air-cooling rate. When the holding temperature is high, the degree of austenitization is high, while the carbon content in the austenite and its stability is reduced during the holding process. Hence, supercooled austenite transforms into granular bainite structure above the upper bainite formation temperature.

Based on the carbon concentration balance in steel, the carbon concentration in martensite can be calculated by utilizing the following formula [11]:

$$C_m = \frac{C_c - C_f(1 - f_m)}{f_m} \quad (1)$$

where C_c and C_f denote the average carbon concentrations of the experimental steel and the ferrite matrix, respectively, f_m is the proportion of the martensite phase, and the ferrite carbon concentration can be computed using thermo-calc thermodynamics software (thermo-calc software Incorporated, Stockholm, Sweden).

The ferrite carbon concentration and the corresponding martensite carbon concentration of the experimental steel at different temperatures were obtained by means of relevant calculation. As illustrated in Table 1, as the austenitizing temperature increases, the percentage of martensite gradually increases, while carbon concentrations in martensite gradually decreases.

Table 1. Microstructure parameters and mechanical properties of LH800 steel at various austenitizing temperatures.

AT/°C	$d_f/\mu\text{m}$	$V_m/\%$	$C_f/\text{wt.}\%$	$C_m/\text{wt.}\%$	HV	YS/MPa	UTS/MPa	UEL/%	TEL/%
750	3.03	39	0.006	0.23	211	344	640	13.3	20.7
775	2.62	48	0.005	0.19	220	385	703	13.1	20.1
800	2.32	56	0.004	0.17	241	423	719	12.5	18.6
825	---	--	0.003	0.16	284	673	897	6.8	13.6

AT: austenitizing temperature; d_f : the grain size of ferrite; V_m : martensite phase proportion; C_f : the carbon concentration of ferrite; C_m : martensitic carbon content; HV: Vickers hardness; YS: yield stress; UTS: tensile stress; UEL: uniform elongation; TEL: total elongation.

3.3. Mechanical Property Analysis

Figure 6 presents the change in the mechanical properties of LH800 steel at various austenitizing temperatures. Figure 6a displays the stress–strain curves of LH800 steel after holding for 15 min at different austenitizing temperatures, followed by air quenching. Notably, LH800 steel exhibited a continuous yield in the tensile process at room temperature. As shown in Figure 6b, the total elongation of 750 °C LH800 steel is the highest, measuring up to 20.7%, and its uniform elongation is also the highest, measuring up to 13.3%. As the temperature increased, the uniform and total elongation decreased accordingly, but when the temperature increased to 825 °C, the uniform and total elongation decreased drastically. Figure 6c exhibits the variations occurring in the strength and hardness of LH800 steel in accordance with changing austenitizing temperatures. The yield strength, tensile strength, and Micro-Vickers hardness of LH800 steel at 750 °C were measured to be the lowest, i.e., 344 MPa, 640 MPa, and 211 (HV), respectively. As temperature increased, the strength and hardness of LH800 steel increased as well. The yield strength, tensile strength, and Vickers hardness of LH800 steel at 825 °C were at its highest, measuring about 673 MPa, 897 MPa, and 284 (HV), respectively. Between 750 and 800 °C, strength and hardness increased slowly, while they increased considerably between 800 and 825 °C; the change trend, the amplitude of microhardness, and yield strength remained relatively consistent. The yield strength and microhardness data in the range of 750–825 °C were fitted linearly, which are exhibited in Figure 6d. The yield strength and Vickers hardness of LH800 steel have a positive correlation, for which its coefficient equals 4.5; that is, the higher the Vickers hardness, the higher the yield strength.

In the range of 750–800 °C, the degree of austenitization increased with increasing temperature, which also induced an increase in the percentage of martensite phase obtained by air quenching. Attributable to the high strength and hardness of martensite, the strength and hardness of LH800 steel also increased in this temperature range. It is known that the plasticity of martensite is poor, while the plasticity of ferrite is good. In the range of 750–800 °C, the percentage of martensite increased gradually, with a gradual decrease in the percentage of ferrite, which eventually led to a decrease in the elongation of LH800 steel in this temperature range.

Between 750 and 800 °C, the matrix is mainly ferrite phase. During the room temperature stretching process, plastic deformation mainly occurred in the ferrite matrix, and a small part of martensite also deformed. Therefore, the increase in strength and the decrease in the plasticity of LH800 steel are not obvious in this temperature range. However, at 825 °C, the matrix is mainly granular bainite. During the plastic deformation process of LH800 steel, an initial deformation occurred in a small amount of ferrite phase, and then high-strength granular bainite was mainly involved in the deformation. Therefore, the strength of LH800 steel increased significantly at this temperature, and plasticity decreased sharply.

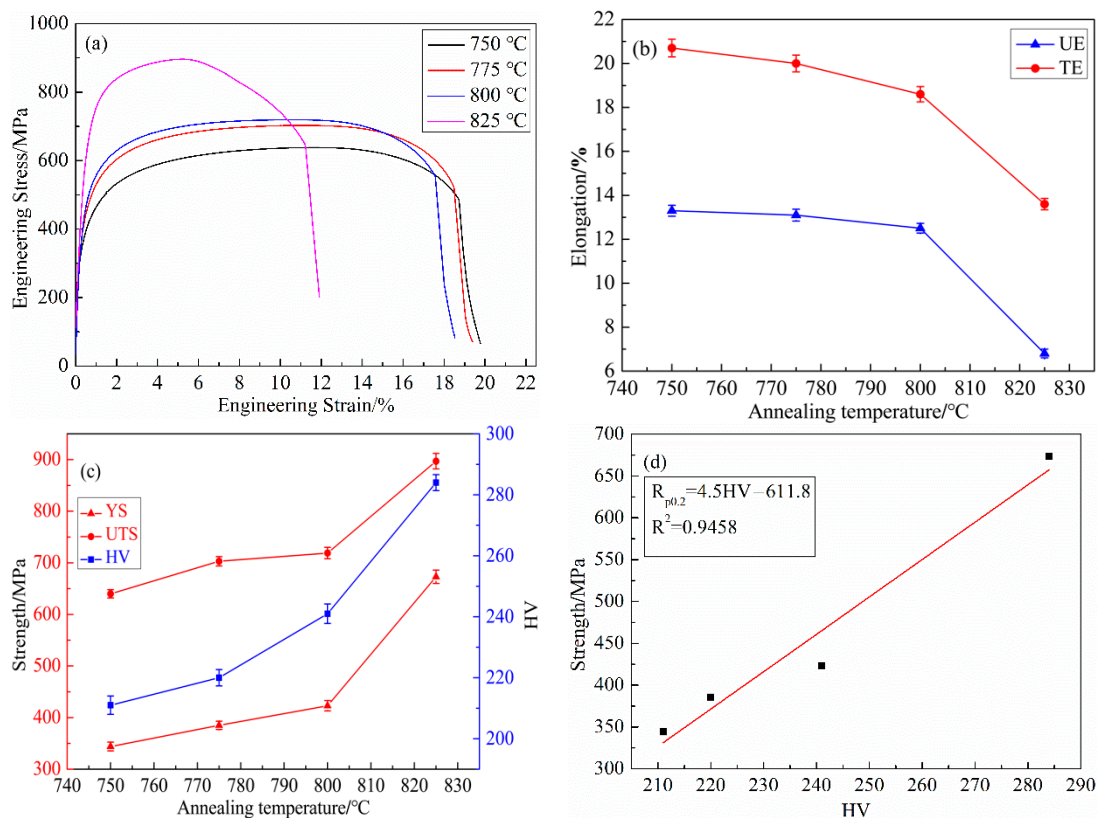


Figure 6. Mechanical properties of LH800 steel at different temperatures for 15 min followed by air quenching. (a) Engineering stress–strain curves of LH800. (b) Changes in elongation of LH800. (c) Changes in yield strength, tensile strength, and Vickers hardness of LH800. (d) The relationship between yield strength and Vickers hardness. (UE: uniform elongation; TE: total elongation; YS: yield stress; UTS: tensile stress; HV: Vickers hardness).

3.4. Work Hardening Analysis

In this paper, we thoroughly evaluated the work hardening characteristics of the LH800 steel during deformation at room temperatures by employing the Hollomon model, differential C-J model, and modified C-J model. These three work-hardening models that describe the associated behavior of the experimental steel are the most prevalent and advanced mathematical analysis models.

3.4.1. Hollomon Analysis

The strain hardening behavior of majority of the metals can be depicted by the Hollomon formula [12]:

$$\sigma = K\varepsilon^n \quad (2)$$

where K denotes the strength coefficient, and n represents the strain hardening exponent. Equation (2) can be expressed as follows.

$$\ln \sigma = \ln K + n \ln \varepsilon \quad (3)$$

In the double logarithmic curve $\ln \sigma - \ln \varepsilon$, the slope of the straight line represents strain-hardening exponent n , and when $\varepsilon = 1$ ($\ln \varepsilon = 0$), and the intercept of the straight line depicts the strength coefficient K . The larger the work hardening index n , the stronger the work hardening ability of the metal, the better the stretch forming performance, and the greater the necking resistance.

Figure 7a shows that the $\ln\sigma$ and $\ln\epsilon$ of LH800 steel are not linear. This indicates that the work hardening behavior of LH800 steel fails to comply with one-stage strain hardening characteristics. However, all the curves of LH800 steel were found to have two fixed slopes, which signifies that the strain hardening behavior of the LH800 steel conforms to two-stage strain hardening characteristics, where ϵ_t is used to represent the transition strain between each deformation stage. Several studies have also reported the two-stage strain hardening characteristics of the DP steel, where a certain plastic deformation was observed to occur in the corresponding microstructure at each stage [13–16]. Table 2 demonstrates that the work hardening index of all the samples in the first stage is larger than that in the second stage. With the increase in deformation degree, the work hardening ability of the specimen decreases correspondingly. Figure 7b illustrates that as the austenitizing temperature increases, the work hardening index of each stage of the samples decreases accordingly, along with a decline in their transition strains, and the plastic deformation of martensite starts earlier.

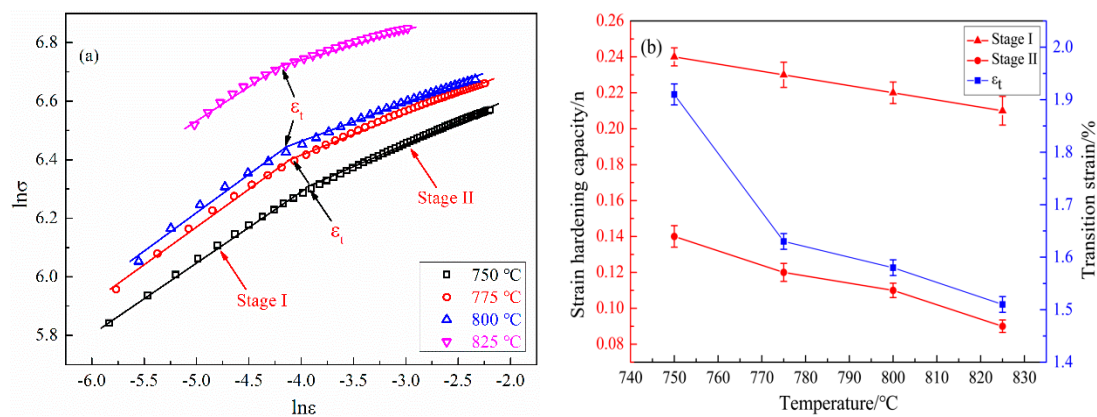


Figure 7. (a) The $\ln\sigma$ vs. $\ln\epsilon$ plots for the Hollomon model of LH800 steel. The slope of the line segment is n ; ϵ_t is the transition strain between each deformation stage. (b) Effect of austenitizing temperature on the work hardening behavior of each stage and the transition strain in the Hollomon model of LH800 steel.

Table 2. Parameters related to the work-hardening behavior in the Hollomon model of LH800 steel.

Austenitizing Temperature/°C	Stage I		Stage II		Transition Strain/%	R-Square
Temperature/°C	n_1	K_1	n_2	K_2	ϵ_t (Stage I–II)	
750	0.24	1413	0.14	965	1.91	0.9989
775	0.23	1500	0.12	1030	1.63	0.9960
800	0.22	1589	0.11	1034	1.58	0.9944
825	0.21	2037	0.09	1266	1.51	0.9927

The appearance of various strain hardening stages in steel is closely related to the activation status of the corresponding deformation mechanism of each stage. In these heat-treated samples, the slope of the first stage is relatively large, reflecting that the strain hardening capacity of the samples in this stage is relatively strong, which is linked to the plastic deformation behavior of ferrite. However, the slopes of the second stage tend to be rather small, indicating that the work hardening ability in this stage is weak, which is related to the common deformation of ferrite and martensite/bainite [17].

Higher austenitizing temperature increases the martensite phase proportion of the LH800 steel, thereby reducing its work hardening ability. It has been reported in existing studies that the work hardening behavior of DP steel is inevitably affected by the ferrite grain size, where the n value of DP steel reduces with a decrease in ferrite grain size [11,18]. Thus, it can be pointed out that the variation of the n value is a result of the change in

the martensite phase proportion and ferrite grain size caused by varying austenitizing temperatures. Table 1 shows that as the austenitizing temperature increases, the martensite phase proportion increases, and ferrite grain size decreases, which eventually results in the reduced strain hardening capacity of LH800 steel at each stage. This implies that the Hollomon analysis model can better explain the multi-stage strain-hardening behavior and plastic deformation mechanism of LH800 steel.

3.4.2. Differential Crussard–Jaoul (D_{C-J}) Analysis

The DC-J model [19,20] used in this paper is based on the Ludwik equation [21]; the Ludwik equation is expressed as follows:

$$\sigma = \sigma_0 + k\varepsilon^n \quad (4)$$

where n is the strain hardening exponent, and σ_0 , and K are the material constants. After using the derivation of strain ε on both sides of Formula (4), we can acquire the following.

$$\ln\left(\frac{d\sigma}{d\varepsilon}\right) = \ln(kn) + (n - 1) \ln \varepsilon \quad (5)$$

DC-J analysis was performed on the tensile data of different heat treatment processes; the results are shown in Figure 8. By fitting the experimental data and performing calculations, the $(n - 1)$ value, the strength coefficient K value, the transition strain ε_t , and the fitting coefficient (R2) of the heat-treated sample were obtained. The calculation results are summarized in Table 3. As shown in Figure 8a, when the austenitizing temperature is 750 °C, the LH800 steel exhibits three-stage strain hardening behavior. Analogous to the previous Hollomon model analysis, the three-stage work hardening behavior of LH800 steel is associated with the deformation mechanism of each stage. According to Zhang et al. [22], the first stage is triggered by the deformation of ferrite phase and the mobile geometrically necessary dislocations (GNDs). The second stage is a result of the uniform deformation of the ferrite phase, while the third stage is effectuated by the co-deformation of ferrite and martensite. As the austenitizing temperature increases, the percentage of martensitic phase increases, the three-stage work hardening behavior of LH800 steel converts to two-stage work hardening behavior. The results indicate that the percentage of martensite phase is instrumental in influencing the work hardening behavior of LH800 steel. Comparing the $(n - 1)$ value and the corresponding transition strain of LH800 steel at each stage at different austenitizing temperatures, it can be found that the $(n - 1)$ value has no correlation with the change in the martensite volume fraction. Overall, DC-J analysis fails to establish the relationship between the microstructure of LH800 steel and its work hardening behavior at each stage.

Table 3. Parameters related to the work-hardening behavior in the D_{C-J} model of LH800 steel.

Austenitizing Temperature/°C	Stage I		Stage II		Stage III		Transition Strain/%		R-Square
	$n_1 - 1$	K_1	$n_2 - 1$	K_2	$n_3 - 1$	K_3	ε_{t1} (Stage I–II)	ε_{t2} (Stage II–III)	
750	−0.45	2063	−1.2	−162	−0.89	1099	0.76	1.72	0.9766
775	−0.72	2177	−1.15	−459	-	-	0.57	-	0.9931
800	−0.86	1823	−1.16	−403	-	-	0.81	-	0.9844
825	−0.09	3365	−1.09	−597	-	-	1.82	-	0.9910

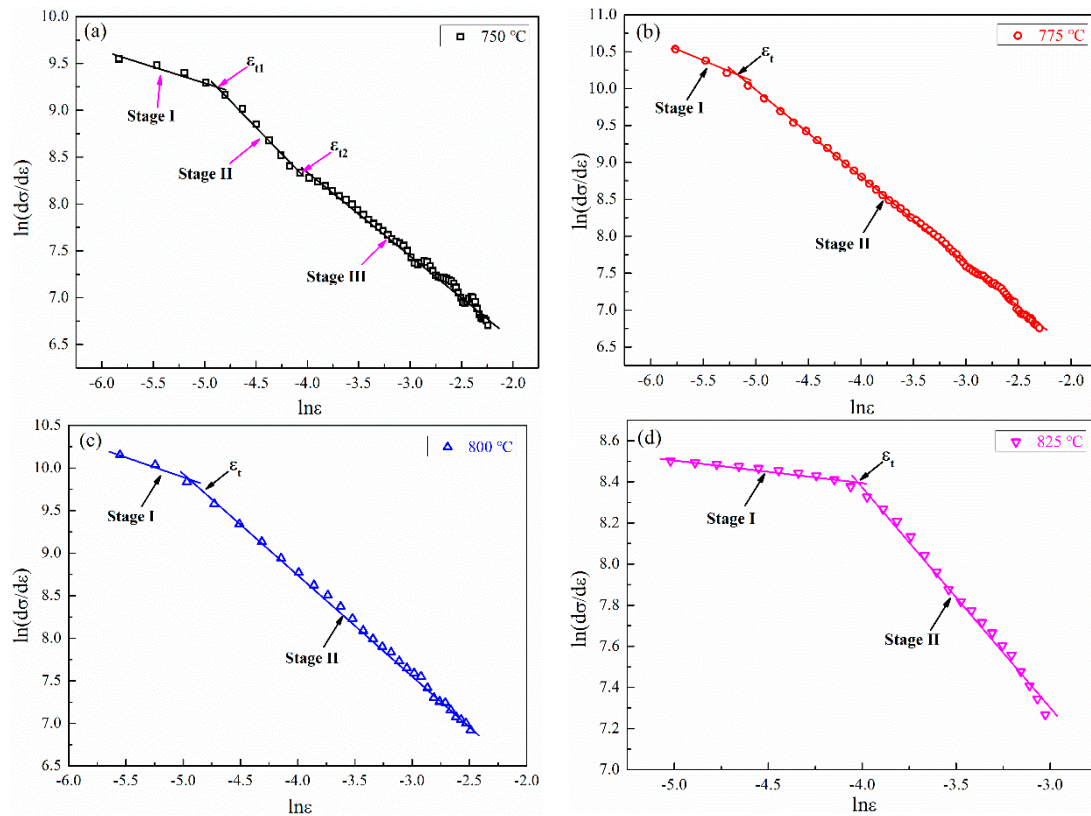


Figure 8. The $\ln(d\sigma/d\varepsilon)$ vs. $\ln\varepsilon$ plots for the $DC\text{-}J$ model of LH800 steel at different austenitizing temperatures: (a) 750 °C; (b) 775 °C; (c) 800 °C; (d) 825 °C.

3.4.3. Modified C-J ($MC\text{-}J$) Analysis

The $MC\text{-}J$ model [20,23,24] is obtained based on the Swift equation [25], which is expressed as follows:

$$\varepsilon = \varepsilon_0 + c\sigma^m \quad (6)$$

where ε_0 and c are material constants, m denotes the reciprocal of the work hardening exponent; after the derivation of σ on both sides of Equation (6), we can obtain the following.

$$\ln\left(\frac{d\sigma}{d\varepsilon}\right) = (1 - m) \ln \sigma - \ln(cm) \quad (7)$$

Figure 9a illustrates the $\ln(d\sigma/d\varepsilon)$ and $\ln\sigma$ curves of LH800 steel at various austenitizing temperatures. Table 4 shows that LH800 steel exhibits three-stage work hardening characteristics at different austenitizing temperatures. The value of m^{-1} indicates the strength of work hardening ability. The larger m^{-1} is, the stronger the work hardening ability of the material [26]. Figure 9b suggests that the value of m^{-1} in the first stage is the largest, indicating that the work hardening ability is the strongest in this stage, which is predominantly concerned with the deformation of ferrite and the movement of GNDs [27–29]. The value of m^{-1} in the second stage is rather small; that is, the work hardening ability is weak in this stage, which could be attributed to the inhibition of ferrite phase deformation by the hard martensite phase [29,30]. In the third stage, the work hardening ability appears to be the weakest, which is primarily linked to the co-deformation of deformed ferrite and martensite [27–30].

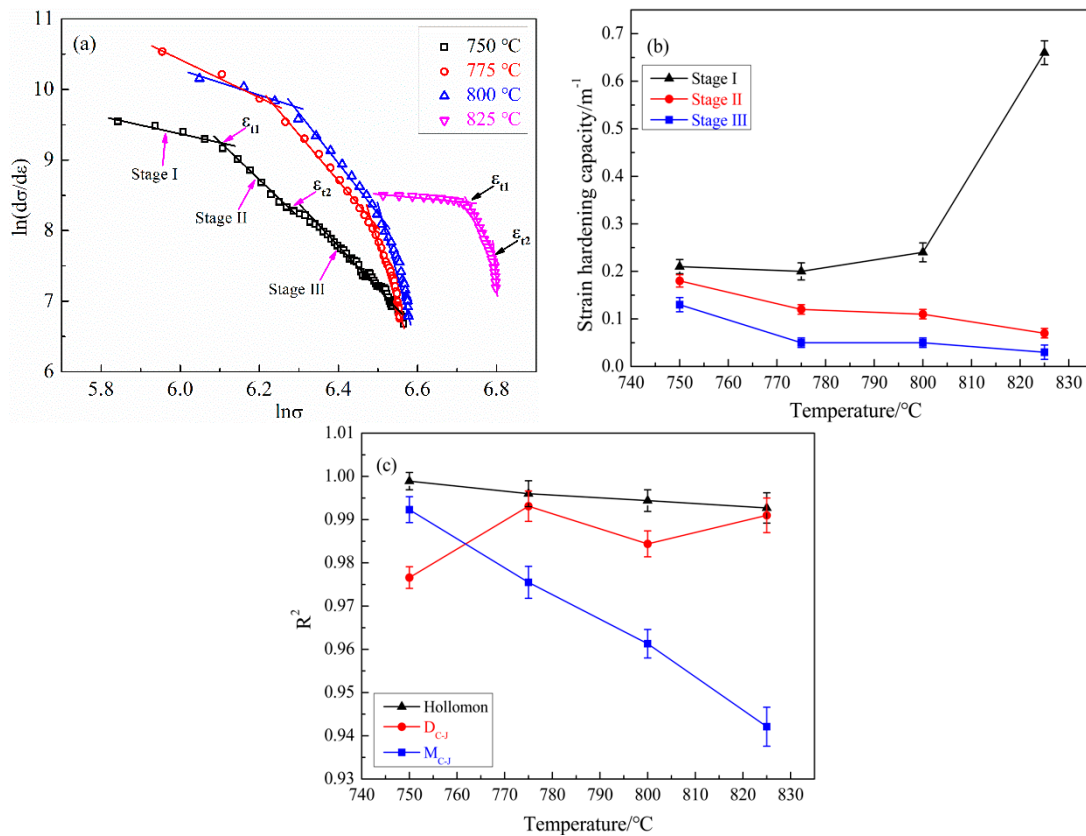


Figure 9. (a) The $\ln(d\sigma/d\epsilon)$ vs. $\ln\sigma$ plots for the M_{C-J} model of the work hardening behavior of LH800 steel. (b) Effect of austenitizing temperature on work hardening ability of LH800 steel in the M_{C-J} model. (c) The correlation coefficients (R^2) of different models vary with austenitizing temperature.

Table 4. Parameters related to the work hardening behavior in M_{C-J} model of LH800 steel.

Austenitizing Temperature/°C	Stage I		Stage II		Stage III		Transition Strain/%		R-Square
	$1 - m_1$	$1/m_1$	$1 - m_2$	$1/m_2$	$1 - m_3$	$1/m_3$	ϵ_{t1} (Stage I-II)	ϵ_{t2} (Stage II-III)	
750	-3.8	0.21	-4.5	0.18	-6.9	0.13	0.84	1.93	0.9923
775	-4.1	0.20	-7.3	0.12	-17.7	0.05	0.83	2.82	0.9755
800	-3.2	0.24	-7.9	0.11	-19.9	0.05	0.81	2.61	0.9613
825	-0.5	0.66	-12.7	0.07	-32.3	0.03	1.62	2.53	0.9421

As austenitizing temperature increases, the percentage of martensite/bainite in LH800 steel increases as well. The inhibition of ferrite deformation by hard phase martensite/bainite is enhanced, and the strain hardening ability of martensite/bainite becomes weaker. The second-stage work hardening behavior is mainly linked to the inhibition of ferrite phase deformation by hard-phase martensite/bainite, which diminishes the second-stage strain hardening ability of LH800 steel. The third-stage work hardening behavior is closely linked to the co-deformation of ferrite phase and hard phase martensite, which also undermines the third-stage strain hardening ability. Figure 9b shows that the experimental results are consistent with the MC-J analysis. Nonetheless, as the austenitizing temperature increases, the percentage of ferrite phase in LH800 steel gradually decreases, and the first-stage work hardening ability is mainly linked to the ferrite phase deformation. Therefore, theoretically, the first-stage work hardening ability should decrease; hence, the result proves to be inconsistent with Figure 9b. This implies that the MC-J model cannot reasonably explain the variation law of the work hardening behavior of LH800 steel.

Figure 9c illustrates the variation of the fitting correlation coefficient (R^2) of different models with varying austenitizing temperatures. The value of R^2 reflects the degree of linear fitting. It can be seen that out of the three employed analysis models, the Hollomon model possesses the largest R^2 value; that is, the Hollomon model exhibits the highest fitting degree. With an increase in austenitizing temperature, the R^2 values of the MC-J model gradually decrease, indicating that their degree of fitting gradually decreases as well, while the R^2 value of the DC-J model continues to fluctuate, indicating that its fitting was unstable.

4. Conclusions

- (1) In this paper, we obtained a low-alloy high-strength steel with ferrite + martensite/bainite structure by conducting partial austenitizing treatment, followed by air quenching. Austenitizing between 750 °C and 800 °C, the typical two-phase structure of ferrite + martensite was obtained by air quenching. The ferrite matrix contains minimal number of carbides. With the increase in austenitizing temperature, there was an increase in the percentage of martensite and a decrease in the ferrite grain size. When the austenitizing temperature reaches 825 °C, the multiphase structure of ferrite + granular bainite + martensite was achieved by air quenching, and the carbides in the ferrite matrix increased as well.
- (2) Between 750 °C and 825 °C, with the increase in austenitizing temperature, the yield strength, tensile strength, and Vickers hardness of LH800 steel increased, while elongation decreased. Yield strength and Vickers hardness have a positive correlation, with the positive correlation coefficient being 4.5. When the temperature increased to 825 °C, LH800 steel exhibited the highest strength and good elongation; its tensile strength was as high as 897 MPa, and elongation was about 13.6%.
- (3) The work hardening behavior of LH800 steel was evaluated using Hollomon, D_{C-J} , and M_{C-J} work hardening models. We found that the Hollomon model is the finest match to the experimental data and can best describe the work hardening behavior of LH800 steel. The work hardening mechanism of LH800 steel is characterized by two-stage strain hardening behavior. The first stage work hardening ability is strong, which is linked to the plastic deformation of ferrite. The second stage work hardening ability is weak, which is linked to the co-deformation of ferrite and martensite/bainite phase. With the increase in austenitizing temperature, there is a gradual decrease in the work hardening ability of LH800 steel at each stage, with a gradual decline in the transition strain, and plastic deformation of martensite starts earlier.

Author Contributions: Conceptualization, X.L.; methodology, X.L., Z.M. and Y.W.; investigation, X.L. and Y.Y.; writing—original draft preparation, X.L.; visualization, H.J. and K.H.; writing—review and editing, X.L. and Z.M.; All authors have read and agreed to the published version of the manuscript.

Funding: This work was financially supported by The National Key R&D Program of China (2021YFB3702404).

Institutional Review Board Statement: Not applicable.

Informed Consent Statement: Not applicable.

Data Availability Statement: The data presented in this study are available upon request from the corresponding author.

Conflicts of Interest: The authors declare no conflict of interest.

References

1. Baudin, T.; Quesne, C.; Jura, J.; Penelle, R. Microstructural characterization in a hot-rolled, two-phase steel. *Mater. Charact.* **2001**, *47*, 365–373. [\[CrossRef\]](#)
2. Nikkhah, S.; Mirzadeh, H.; Zamani, M. Fine tuning the mechanical properties of dual phase steel via thermomechanical processing of cold rolling and intercritical annealing. *Mater. Chem. Phys.* **2019**, *230*, 1–8. [\[CrossRef\]](#)

3. Zhang, F.; Ruimi, A.; Wo, P.C.; Field, D. Morphology and distribution of martensite in dual phase (DP980) steel and its relation to the multiscale mechanical behavior. *Mater. Sci. Eng. A* **2016**, *659*, 93–103. [[CrossRef](#)]
4. Schmitt, J.H.; Lung, T. New developments of advanced high-strength steels for automotive applications. *Comptes Rendus Phys.* **2018**, *19*, 641–656. [[CrossRef](#)]
5. Balbi, M.; Alvarez-Armas, I.; Armas, A. Effect of holding time at an intercritical temperature on the microstructure and tensile properties of a ferrite-martensite dual phase steel. *Mater. Sci. Eng. A* **2018**, *733*, 1–8. [[CrossRef](#)]
6. Zhang, M.D.; Hu, J.; Cao, W.Q.; Dong, H. Microstructure and mechanical properties of high strength and high toughness micro-laminated dual phase steels. *Mater. Sci. Eng. A* **2014**, *618*, 168–175. [[CrossRef](#)]
7. Grydin, O.; Rodman, D.; Schaper, M. Influence of cold forming and heat treatment on the microstructure and mechanical properties of an air-hardening steel. *Steel Res. Int.* **2012**, *83*, 1020–1028. [[CrossRef](#)]
8. Schaper, M.; Grydin, O.; Nürnbergger, F. Microstructure evolution of the air-hardening steel LH800® due to heat treatment. *HTM J. Heat Treat. Mater.* **2013**, *68*, 42–48. [[CrossRef](#)]
9. Grydin, O.; Nuernberger, F.; Zou, Y.; Schaper, M.; Brosius, A. Formation and properties of mixed ferritic-martensitic microstructures in the air-hardening steel LH800. *Steel Res. Int.* **2014**, *85*, 1340–1347. [[CrossRef](#)]
10. Wolf, L.; Nürnbergger, F.; Rodman, D.; Maier, H.J. The effect of intercritical annealing on the microstructure and mechanical properties of ferritic-martensitic two-phase steels. *Steel Res. Int.* **2017**, *88*, 1600107. [[CrossRef](#)]
11. Calcagnotto, M.; Adachi, Y.; Ponge, D.; Raabe, D. Deformation and fracture mechanisms in fine- and ultrafine-grained ferrite/martensite dual-phase steels and the effect of aging. *Acta Mater.* **2011**, *59*, 658–670. [[CrossRef](#)]
12. Hollomon, J.H. Time-temperature relations in tempering steel. *Trans. AIME* **1945**, *162*, 223–249.
13. Ramos, L.F.; Matlock, D.K.; Krauss, G. On the deformation behavior of dual-phase steels. *Metall. Trans. A* **1979**, *10*, 259–261. [[CrossRef](#)]
14. Jiang, Z.; Guan, Z.; Lian, J. The relationship between ductility and material parameters for dual-phase steel. *J. Mater. Sci.* **1993**, *28*, 1814–1818. [[CrossRef](#)]
15. Lian, J.; Jiang, Z.; Liu, J. Theoretical model for the tensile work hardening behaviour of dual-phase steel. *Mater. Sci. Eng. A* **1991**, *147*, 55–65. [[CrossRef](#)]
16. Mazaheri, Y.; Kermanpur, A.; Najafzadeh, A. A novel route for development of ultrahigh strength dual phase steels. *Mater. Sci. Eng. A* **2014**, *619*, 1–11. [[CrossRef](#)]
17. Movahed, P.; Kolahgar, S.; Marashi, S.; Pouranvari, M.; Parvin, N. The effect of intercritical heat treatment temperature on the tensile properties and work hardening behavior of ferrite-martensite dual phase steel sheets. *Mater. Sci. Eng. A* **2009**, *518*, 1–6. [[CrossRef](#)]
18. Mazaheri, Y.; Jahanara, A.H.; Sheikhi, M.; Kalashami, A.G. High strength-elongation balance in ultrafine grained ferrite-martensite dual phase steels developed by thermomechanical processing. *Mater. Sci. Eng. A* **2019**, *761*, 138021. [[CrossRef](#)]
19. Monteiro, S.N.; Reed-Hill, R.E. On the double-n behavior of iron. *Metall. Trans.* **1971**, *2*, 2947–2948. [[CrossRef](#)]
20. Umamoto, M.; Tsuchiya, K.; Liu, Z.G.; Sugimoto, S. Tensile stress-strain analysis of single-structure steels. *Metall. Mater. Trans. A* **2000**, *31*, 1785–1794. [[CrossRef](#)]
21. Das, D.; Chattopadhyay, P.P. Influence of martensite morphology on the work-hardening behavior of high strength ferrite-martensite dual-phase steel. *J. Mater. Sci.* **2009**, *44*, 2957–2965. [[CrossRef](#)]
22. Zhang, J.; Di, H.; Deng, Y.; Misra, R.D.K. Effect of martensite morphology and volume fraction on strain hardening and fracture behavior of martensite-ferrite dual phase steel. *Mater. Sci. Eng. A* **2015**, *627*, 230–240. [[CrossRef](#)]
23. Samuel, F.H. Tensile stress-strain analysis of dual-phase structures in an Mn-Cr-Si steel. *Mater. Sci. Eng.* **1987**, *92*, L1–L4. [[CrossRef](#)]
24. Jiang, Z.; Lian, J.; Chen, J. Strain hardening behaviour and its relationship to tensile mechanical properties of dual phase steel. *Mater. Sci. Technol.* **1992**, *8*, 1075–1081. [[CrossRef](#)]
25. Swift, H.W. Plastic instability under plane stress. *J. Mech. Phys. Solids* **1952**, *1*, 1–18. [[CrossRef](#)]
26. Reed-Hill, R.E.; Cribb, W.R.; Monteiro, S.N. Concerning the analysis of tensile stress-strain data using $\log d\sigma/d\epsilon_p$ versus $\log \sigma$ diagrams. *Metall. Trans.* **1973**, *4*, 2665–2667. [[CrossRef](#)]
27. Ramazani, A.; Mukherjee, K.; Schwedt, A.; Goravanchi, P.; Prahl, U.; Bleck, W. Quantification of the effect of transformation-induced geometrically necessary dislocations on the flow-curve modelling of dual-phase steels. *Int. J. Plast.* **2013**, *43*, 128–152. [[CrossRef](#)]
28. Tan, X.; Xu, Y.; Yang, X.; Wu, D. Microstructure-properties relationship in a one-step quenched and partitioned steel. *Mater. Sci. Eng. A* **2014**, *589*, 101–111. [[CrossRef](#)]
29. Ahmad, E.; Manzoor, T.; Hussain, N. Thermomechanical processing in the intercritical region and tensile properties of dual-phase steel. *Mater. Sci. Eng. A* **2009**, *508*, 259–265. [[CrossRef](#)]
30. Xiong, Z.P.; Kostryzhev, A.G.; Stanford, N.E.; Pereloma, E.V. Microstructures and mechanical properties of dual phase steel produced by laboratory simulated strip casting. *Mater. Des.* **2015**, *88*, 537–549. [[CrossRef](#)]